

AN IMPROVED OPTOFLUIDIC MICROSCOPE

Mozziyar Etemadi¹, Shivonne Haniff², and Saket Vora¹

Departments of ¹Electrical and ²Mechanical Engineering, Stanford University
Stanford, California

Abstract. Optofluidic microscopy (OFM) is an emerging technique for high-resolution optical imaging for organisms in a compact form-factor. Utilizing a lensless shadow imaging method with a CMOS image sensor and augmented with aperture-based raster-scanning, images of *C. elegans* of similar quality to 20x conventional microscopy have been attained with a resolution of approximately 1µm [1]. Previous improvements to OFM have included more robust raster-scanning techniques and adding a Fresnel lens layer [2]. Building upon the former, we propose obtaining higher SNR images by increasing the integration time. This requires integrating flow sensors to better measure the flow speed. This feature, along with multiple linear aperture arrays, will enable more accurate image construction. We determined an improved integration time for the sensor, which is 30-50 ms, enhancing the SNR of the resolved image by over 15 dB. Replacing the aperture grid material with amorphous silicon and standard etch processes allowed for in-line integration of piezoresistive differential pressure sensors under the microfluidic channel to measure fluid flow.

Background. Amidst the multitude of microscopy techniques, optical imaging of cells and organisms remains an important tool in biology and pathology [3], especially for point-of-care testing (POCT) [4]. One approach taken to miniaturize optical microscopy for portability is OFM, which can be entirely implemented on-chip. A slanted linear array of apertures is placed above a CMOS image sensor and specimens are flowed above the apertures in a PDMS microfluidic channel while being illuminated from above [5]. A raster-scan shadow image of the specimen is obtained as it flows across the apertures, to a resolution of ~0.8µm. This is comparable to conventional microscopy resolutions of ~0.2µm to 1µm, depending on wavelength [3]. Other approaches to microfluidic imaging and identification of cells include fluorescence-based sensing such as µFACS [6], absorbance, chemiluminescence [7], rigidity sensing for malaria [8], LUCAS [9], and more. Many of these, particularly the fluorescence-activated ones, are geared towards efficient cell-sorting [10-11], where the parameter in question is dyed or tagged with a fluorescence marker. Optical image quality is sacrificed for higher throughput and sorting efficiency, but in some diagnoses of blood parasites, water quality, and urine analysis [12], image quality is more critical than quantitative analysis.

Yang *et al* design. First, the image quality is limited by the SNR of the CMOS imager. Second, the Yang *et al* device requires a constant flow rate and fails if the sample rotates or deviates from a straight-line path due to image distortion. Yang *et al* reported rejection rates of up to 45% —rendering the device unusable in a field setting where the amount of sample is limited and difficult to obtain. Finally, the aperture grid is created by boring into the aluminum layer using a focused-ion-beam which is not suitable for mass production. With regards to improving SNR, we examine the equation for the SNR of a CMOS image sensor [13]:

$$SNR = 10 \log_{10} \left(\frac{(i_{ph} t_{int})^2}{(q(i_{ph} + i_{dc})t_{int} + q^2(\sigma_{read}^2 + \sigma_{DSNU}^2) + (\sigma_{PRNU} i_{ph} t_{int})^2)} \right)$$

The numerator term is the “signal” and is proportional to the square of the photocurrent and the integration time (shutter speed). The photocurrent is equal to the light intensity (typically given in mW/cm²) multiplied by the effective cross sectional area of the aperture, multiplied by the photoresponsivity of the material (roughly 0.6 for silicon). The denominator consists of three terms: the first is the shot noise of both the photo and dark current, the second term is thermal noise, and the final term is “fixed pattern noise” due to slight mismatches between each pixel (caused by minute fabrication errors). The reader should note that as the shutter time approaches infinity, the SNR is limited by the inverse of fixed pattern noise. This is typically quite small, leading to a large SNR. Shot and fixed pattern noise are inherent to the sensor fabrication process, so to increase the SNR we must either increase light intensity or integration time. Increasing light intensity is problematic because it will either heat up the sample or exceed the dynamic range of the CMOS pixels. Thus, we are left with integration time. A consequence of increasing the integration time is a decrease in flow rate, and thus the total time needed to obtain an image. Assuming an integration time t_{int} and apertures of radius r , the flow rate needed such that a particular part of the sample remains over a single aperture for the entire integration time is $F = 2r/t_{int}$. Note that this flow rate is given in terms of distance/time, *not* volumetric flow rate. The total time to image the sample is simply the length of the entire array of apertures plus the length of the organism, all divided by

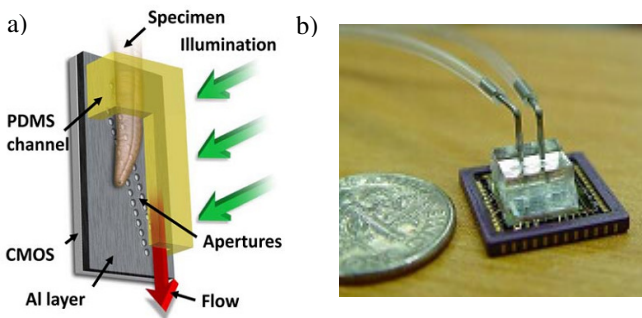


Figure 1. (a) OFM system proposed by Yang *et al* (only 1 row of apertures implemented) [1]. (b) Miniaturization potential of OFM by Yang *et al* [5]. This size is ideal for POCT and field applications.

In this paper, we explore improvements to the OFM approach outlined by Yang *et al* and Salama *et al* to increase its performance, as outlined below.

Design. We see at least three fundamental improvements in the

this flow rate. The longer acquisition time exacerbates both the necessity to keep a constant flow rate and the need to compensate for sample rotations or deviations over the longer time period. Irregularities in flow rate are minor if a large external pumping system is used, but is problematic for handheld use, i.e. with a syringe. Thus, we propose integration of a flow sensor into the design such that flow rates could be measured in real-time to correct for rate irregularities. To address the problem of sample rotation, we propose adding extra apertures to record multiple versions of the same image and aiding in deskewing, similar to Salama, *et al.* Finally, we propose that the new aperture array and flow sensor be built using all standard CMOS as to facilitate mass production of the device.

Fabrication. The OFM device uses a 2D CMOS imaging sensor with electrodes separating each $0.9\mu\text{m} \times 9.9\mu\text{m}$ sensor pixel (Fig. 2a). A $2\mu\text{m}$ layer of SU8 photoresist is spun over the CMOS sensor to planarize the surface. An amorphous silicon (a-Si) layer of 300 nm is then deposited onto the SU8 to mask the CMOS pixels from light (Fig. 2b). Nanoimprint lithography is utilized to pattern the aperture holes [14]. A SiO_2 mold with cylindrical structures is pressed into a thin layer of PMMA (Fig. 2c). The Reactive Ion Etching (RIE) process is used to create the $1\mu\text{m}$ diameter apertures (Fig. 2d). The PMMA is stripped and a different SU8 mask is formed (Fig. 2e) to create the grooves (Fig. 2f) for the pressure sensors using RIE. The mask is etched away and the a-Si diaphragm pressure sensors (process outlined by Ishihara *et al.*) [15] are created within the grooves formed in the a-Si layer. A $0.2\mu\text{m}$ layer of PMMA is spin-coated on top of the a-Si layer to protect the OFM apertures and sensors. A PDMS microfluidic chip with a channel is formed by injection molding [16] and then bonded to the a-Si coated CMOS sensor with a Suss Mask aligner (Fig. 2g). Finally, press-fit holes are bored with a modified needle into the inlet and outlet of the PDMS channel. Standard tubing is then connected to the needle. These interconnects can be disassembled and reassembled without affecting the seal [17].

Analysis of Performance. The improvement in SNR is quantified below, as well as the expected full image acquisition times and flow rates associated with each SNR value. First, we look at flow rates. We choose various integration times, and assuming we have a $200\mu\text{m}$ long sample travelling across 20 apertures ($1\mu\text{m}$ diameter) with $10\mu\text{m}$ vertical spacing, we obtain the results in Table 1.

| Int. time (ms) | Max flow rate (cm/min) | Total Acq. Time (s) |
|----------------|------------------------|---------------------|
| 1 | 6 | 0.4 |
| 5 | 1.2 | 2 |
| 10 | 0.6 | 4 |
| 30 | 0.2 | 12 |
| 50 | 0.12 | 20 |
| 100 | 0.06 | 40 |

Table 1 – Max flow rate and acquisition time for varying integration times.

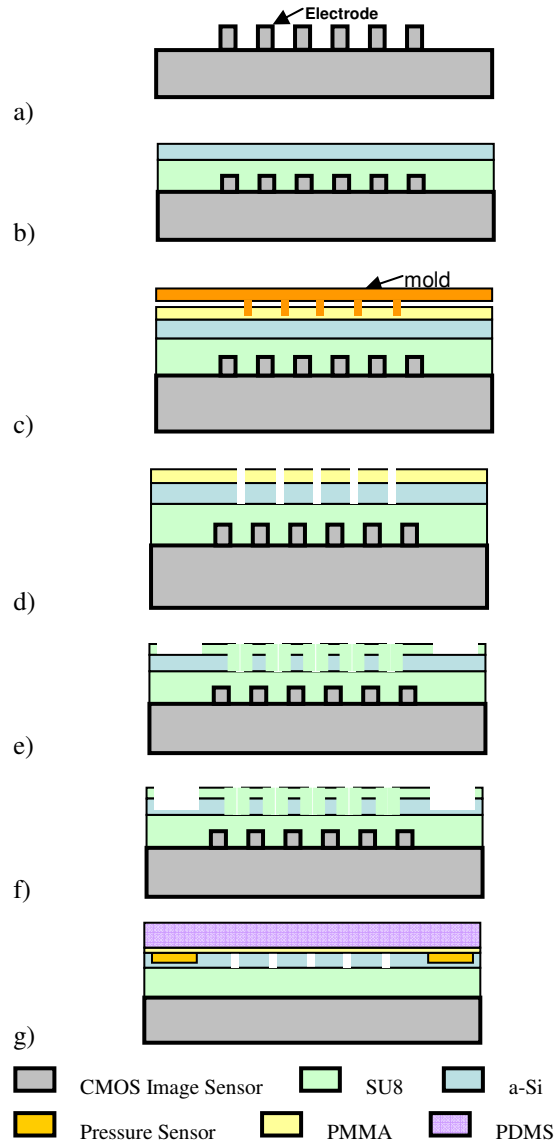


Figure 2. Side view of process steps.

The SNR expected at various intensities of illumination and shutter speeds is shown in Figure 3.

Finally, the results are combined to depict the SNR as a function of the total acquisition time. We choose an illumination current of 1×10^{14} A, same as the one used in the work by Yang *et al.*

The Yang *et al.* device, with its 1ms shutter speed corresponding to a total acquisition time of 0.4 seconds, achieves an SNR of less than 15 dB. By increasing the acquisition time to 20 seconds—still within a reasonable time limit for a clinical setting—the SNR increases to over 30 dB. As we mentioned, increasing the total acquisition time also requires that the flow rate remain constant for this time period and that rotation be accounted for. Since we are now also recording the flow rate, the first requirement is gone, and the multiple apertures remove the second requirement.

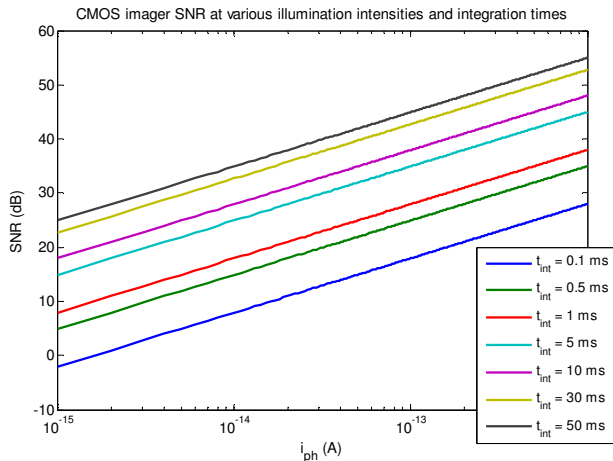


Figure 3. SNR for CMOS imager at various illumination intensities and integration times.

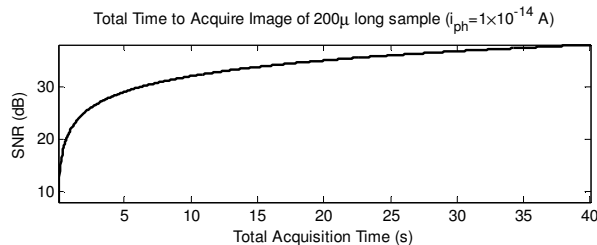


Figure 4. SNR for different acquisition times for a 200µ sample.

Conclusions. We have optimized the integration time of the OFM device to achieve a higher SNR image. We have addressed the need for better regulation of flow rate with an integrated flow sensor, and accounted for sample deviations using an array of apertures. Additionally, we have modified the fabrication process to employ standard CMOS processing, further enabling mass production. These improvements push the OFM technique closer to a POCT environment. Future work needs to address increased resolution (with smaller apertures), quantitative measurements derived from the OFM images, and on-chip preparation and handling of samples, i.e. staining and temperature regulation. Further experiments should use more representative samples such as blood, urine, and contaminated water.

References.

[1] X. Cui, L. M. Lee, X. Heng, W. Zhong, P. W. Sternberg, D. Psaltis, and C. Yang, "Lensless high-resolution on-chip optofluidic microscopes for caenorhabditis elegans and cell imaging." *Proceedings of the National Academy of Sciences of the United States of America*, vol. 105, no. 31, pp. 10 670-10 675, August 2008. [Online]

[2] J. Wu, X. Cui, L. M. Lee, and C. Yang, "The application of fresnel zone plate based projection in optofluidic microscopy," *Opt. Express*, vol. 16, no. 20, pp. 15 595-15 602, 2008. [Online].

[3] Y. Garini, B. Vermolen, and I. Young, "From micro to nano: recent advances in high-resolution microscopy," *Current Opinion in Biotechnology*, vol. 16, no. 1, pp. 3-12, February 2005. [Online].

[4] M. J. Pugia, G. Blankenstein, R.-P. Peters, J. A. Profitt, K. Kadel, T. Willms, R. Sommer, H. H. Kuo, and L. S. Schulman, "Microfluidic tool box as technology platform for hand-held diagnostics," *Clin Chem*, vol. 51, no. 10, pp. 1923-1932, October 2005. [Online].

[5] X. Cui, X. Heng, and C. Yang, "Optofluidic microscope: a complete on-chip imaging device," D. L. Farkas, D. V. Nicolau, and R. C. Leif, Eds., vol. 6859, no. 1. SPIE, 2008.

[6] B. Yao, G.-A. Luo, X. Feng, W. Wang, L.-X. Chen, and Y.-M. Wang, "A microfluidic device based on gravity and electric force driving for flow cytometry and fluorescence activated cell sorting," *Lab Chip*, vol. 4, no. 6, pp. 603-607, 2004. [Online].

[7] B. Kuswandi, Nuriman, J. Huskens, and W. Verboom, "Optical sensing systems for microfluidic devices: a review." *Anal Chim Acta*, vol. 601, no. 2, pp. 141-155, October 2007. [Online].

[8] R. Zhang, "Application of microfluidic device to malaria diagnosis," Ph.D. dissertation, MIT, August 2007.

[9] S. Seo, T.-W. Su, A. Erlinger, and A. Ozcan, "Multi-color LUCAS: Lensfree on-chip cytometry using tunable monochromatic illumination and digital noise reduction," *Cellular and Molecular Bioengineering*, vol. 1, no. 2, pp. 146-156, 2008. [Online].

[10] K. Chung, M. M. Crane, and H. Lu, "Automated on-chip rapid microscopy, phenotyping and sorting of c. elegans," *Nature Methods*, vol. 5, no. 7, pp. 637-643, June 2008. [Online].

[11] F. Zeng, C. B. Rohde, and M. F. Yanik, "Sub-cellular precision on-chip small-animal immobilization, multi-photon imaging and femtosecond-laser manipulation," *Lab Chip*, vol. 8, no. 5, pp. 653-656, 2008. [Online].

[12] T. A. Elkhatib, Z. Huang, and K. N. Salama, "Real time optofluidic microscopy," in *Circuits and Systems and TAISA Conference, 2008. NEWCAS-TAISA 2008. 2008 Joint 6th International IEEE Northeast Workshop on*, 2008, pp. 53-56. [Online].

[13] El Gamal and H. Eltoukhy, "CMOS Image sensors," *Circuits and Devices Magazine, IEEE*, vol. 21, no. 3, pp. 6-20, 2005. [Online].

[14] S. Y. Chou, P. R. Krauss, and P. J. Renstrom, "Nanoimprint lithography," *Journal of Vacuum Science Technology*, vol. 14, no. 6, pp. 4129+, November 1996.

[15] T. Ishihara, K. Suzuki, S. Suwazono, M. Hirata, and H. Tanigawa, "Cmos integrated silicon pressure sensor," *Solid-State Circuits, IEEE Journal of*, vol. 22, no. 2, pp. 151-156, 1987. [Online].

[16] P. Grodzinski, R. H. Liu, B. Chen, J. Blackwell, Y. Liu, D. Rhine, T. Smekal, D. Ganser, C. Romero, H. Yu, T. Chan, and N. Kroutchinina, "Development of plastic microfluidic devices for sample preparation," *Biomedical Microdevices*, vol. 3, no. 4, pp. 275-283, December 2001. [Online].

[17] M. Christensen, A. Chang-Yen, and K. Gale, "Characterization of interconnects used in PDMS microfluidic systems," *Journal of Micromechanics and Microengineering*, vol. 15, no. 5, pp. 928-934, May 2005. [Online].